

# Information-Thermodynamic Analysis of the DNA–RNA Polymerase Complex via Interface Dissipation: Based on Observer–Observed Swap Symmetry

Tatsuaki Tsuruyama<sup>\*1,2</sup>

<sup>1</sup>Department of Physics, Tohoku University, Sendai 980-8578, Japan

<sup>2</sup>Department of Drug Discovery Medicine, Kyoto University, Kyoto 606-8501, Japan

January 14, 2026

## Abstract

RNA polymerase (RNAP) is a molecular machine that reads information encoded in the base sequence of a DNA template while producing mechanical motion (transcription elongation; forward/backward stepping; backtracking) through chemical-potential differences of nucleoside triphosphates (NTPs) and fluctuations under external conditions. A prior work formulated a mismatch in free-energy accounting as the involvement of a term originating from genetic information (e.g.  $k_B T \log P(N)$ ), and interpreted RNAP as a Maxwell’s demon / Szilard-engine-like device that converts information into motion. However, in information thermodynamics, the bookkeeping of information and dissipation can depend on how one partitions the composite system into a device and a target (observer/observed labeling).

In this manuscript, we apply the swap-symmetric invariant *interface dissipation* to a concrete model of the DNA–RNAP complex. We describe a bipartite system  $(X, Y)$  consisting of template-side degrees of freedom  $X$  and RNAP-side degrees of freedom  $Y$  as a continuous-time Markov jump process, and introduce the joint dissipation  $\Sigma_{XY}$ , marginal dissipations  $\Sigma_X, \Sigma_Y$ , and the swap-invariant interface dissipation

$$\Sigma_{\text{int}} := \Sigma_{XY} - \frac{1}{2}(\Sigma_X + \Sigma_Y).$$

$\Sigma_{\text{int}}$  extracts the irreversibility of conditional fluctuations generated by the interface itself, independently of labeling, and provides a quantitative indicator of dissipation components arising from coupling between sequence-dependent kinetics and chemical driving, such as sequence-dependent rates, misincorporation, backtracking, and proofreading cycles. We also present a practical protocol to estimate  $\Sigma_{\text{int}}$  from single-molecule measurements (step sequences, dwell times, sequence-dependent rates; if needed, inference of internal states via an HMM), and we organize the relation to earlier mutual-information (mutual-entropy) free-energy bookkeeping as *interface dissipation + gauge-dependent conventions*.

## 1 Introduction

### 1.1 RNAP and information thermodynamics: positioning relative to prior work

RNA polymerase (RNAP) is an enzyme that elongates an RNA chain while moving along a DNA template one base (or one effective step) at a time. Single-molecule experiments have enabled high-time-resolution observations of RNAP fluctuations such as stepping, pausing, and backtracking, advancing quantitative understanding of mechanistic and thermodynamic costs of transcription elongation (representative examples include [9, 10, 11, 12, 13, 14]).

A previous work [7] described RNAP forward/backward step fluctuations and the involvement of DNA-base statistics using a state function  $P(m, d, N)$  (position  $m$ , direction label  $d$ , base species

---

<sup>\*</sup>tsuruyam@kuhp.kyoto-u.ac.jp

$N$ ), and showed that a mismatch in estimated free-energy changes can be understood as a difference in how one incorporates a “direction-fluctuation term” and a “sequence-information term” (e.g.  $k_B T \log P(N)$ ). In addition, a review-style draft proposed an interpretation in which two residues in the catalytic domain are regarded as an *Engine* and a *Memory*, and DNA-base information (mutual entropy) is converted into self-motion in a Maxwell-demon-like picture [8].

## 1.2 Partition dependence and interface dissipation

In information thermodynamics, the bookkeeping of information and dissipation can change depending on where one draws the boundary between the “device” and the “target (observed system).” In our axiomatic framework, irreversibility is defined at the first-principles level as a path-space KL divergence, which allows one to distinguish dissipation that is invariant under changes of coarse-graining/coding conventions from gauge-dependent bookkeeping. For a composite system  $(X, Y)$ , we incorporate the observer/observed labeling itself as a swappable degree of freedom and introduce the swap-symmetric invariant called interface dissipation  $\Sigma_{\text{int}}$  [1]. In this manuscript, we apply  $\Sigma_{\text{int}}$  to the DNA–RNAP complex with the aims of:

1. extracting and quantifying, independently of labeling, irreversibility generated by coupling between sequence reading and chemical driving;
2. providing practical guidance to estimate  $\Sigma_{\text{int}}$  from single-molecule data (step sequences, dwell times, and sequence information);
3. reinterpreting prior free-energy accounting via mutual entropy [7, 8] within a higher-level structure of “interface dissipation + gauge choice.”

## 2 General framework of interface dissipation (key points)

### 2.1 Path measures and first-principles definition of dissipation

Let  $P_{XY}$  be the forward path measure of the composite system  $(X, Y)$ . Using the time-reversal map  $\mathcal{R}$ , define the reverse path measure by

$$P_{XY}^{\text{R}} := P_{XY} \circ \mathcal{R}^{-1}. \quad (1)$$

Define irreversibility (dissipation) at the first-principles level as the path-space KL divergence:

$$\Sigma_{XY} := D_{\text{KL}}\left(P_{XY} \parallel P_{XY}^{\text{R}}\right) = \int \log\left(\frac{dP_{XY}}{dP_{XY}^{\text{R}}}\right) dP_{XY}. \quad (2)$$

Let the projections be  $\Pi_X(x, y) = x$ ,  $\Pi_Y(x, y) = y$ , and define  $P_X = \Pi_X P_{XY}$ ,  $P_Y = \Pi_Y P_{XY}$  and  $P_X^{\text{R}} = \Pi_X P_{XY}^{\text{R}}$ ,  $P_Y^{\text{R}} = \Pi_Y P_{XY}^{\text{R}}$ . Then the subsystem dissipations are

$$\Sigma_X := D_{\text{KL}}\left(P_X \parallel P_X^{\text{R}}\right), \quad \Sigma_Y := D_{\text{KL}}\left(P_Y \parallel P_Y^{\text{R}}\right). \quad (3)$$

By the data-processing inequality,  $\Sigma_{XY} \geq \Sigma_X, \Sigma_Y$ .

### 2.2 Interface dissipation and directional component

**Definition 1** (Interface dissipation).

$$\Sigma_{\text{int}} := \Sigma_{XY} - \frac{1}{2}(\Sigma_X + \Sigma_Y) \quad (4)$$

is called the interface dissipation.

$\Sigma_{\text{int}}$  is invariant under swapping  $X \leftrightarrow Y$ , and satisfies  $\Sigma_{\text{int}} \geq 0$  (the swap-symmetric second law) [1]. Introducing the swap-odd directional component

$$\mathcal{J}_{X \rightarrow Y} := (\Sigma_{XY} - \Sigma_X) - (\Sigma_{XY} - \Sigma_Y) = \Sigma_Y - \Sigma_X, \quad (5)$$

hidden dissipation can be decomposed into even/odd parts.

When the conditional path measures  $P_{Y|X}$ ,  $P_{X|Y}$  and their reverse counterparts exist, one has

$$\Sigma_{\text{int}} = \frac{1}{2} \left[ \int D_{\text{KL}} \left( P_{Y|X=\gamma} \middle\| P_{Y|X=\gamma}^{\text{R}} \right) P_X(d\gamma) + \int D_{\text{KL}} \left( P_{X|Y=\eta} \middle\| P_{X|Y=\eta}^{\text{R}} \right) P_Y(d\eta) \right], \quad (6)$$

showing that interface dissipation is the average (from both sides) of the irreversibility of fluctuations conditioned on the partner [1].

*Remark 2* (How we use it in this manuscript). In DNA–RNAP systems, one often considers a limit in which the DNA appears nearly static. Even in that limit, interface dissipation can remain nontrivial due to sequence dependence, proofreading processes, binding/unbinding, etc. In this manuscript, we make explicit how we choose  $X$  (sequence class, base identity, local structure, etc.) and  $Y$  (position, translocation register, chemical state, backtracking, etc.), and we organize the correspondence between observables and  $\Sigma_{\text{int}}$ .

### 2.3 Minimal Brownian-ratchet model: spontaneous fluctuations + locking/rectification by the correct rNTP

In this section, we formalize, as a continuous-time Markov jump process (CTMC), the mechanism emphasized in [7]: RNAP undergoes spontaneous forward/backward fluctuations due to DNA structure, and binding/polymerization of the correct rNTP suppresses backward motion by capturing the post state, thereby realizing an effective forward progression. The crucial point is not that polymerization free energy directly pushes RNAP forward as a mechanical force, but that chemical reactions *lock and rectify* mechanical fluctuations (a Brownian ratchet).

#### 2.3.1 Template (fixed) and interface variable $X_t$

Assume the DNA sequence is a quenched fixed string  $\mathbf{x} = (x_1, \dots, x_L)$ ,  $x_m \in \{A, C, G, T\}$ . We define the template-side stochastic process as

$$X_t := x_{m_t+1}. \quad (7)$$

That is, the *next base to be incorporated* is treated as the interface input  $X_t$ . Even if the DNA itself is fixed, the RNAP position  $m_t$  fluctuates, so  $X_t$  becomes a stochastic process. In this way, “RNAP advances while reading nucleic-acid information” is expressed as a precise probabilistic statement.

#### 2.3.2 RNAP-side state space $Y_t$ : pre/post fluctuations and binding of the correct rNTP

Define the RNAP-side process by

$$Y_t := (m_t, z_t, b_t) \in \mathcal{Y}. \quad (8)$$

Here,

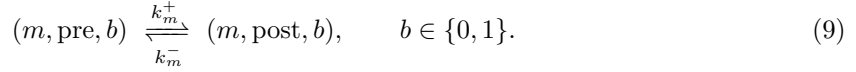
- $m_t \in \{1, \dots, L\}$  is the transcription position (corresponding to  $m$  in [7]),
- $z_t \in \{\text{pre, post}\}$  is the intra-base translocation register (mechanical state),
- $b_t \in \{0, 1\}$  is the binding state of the *correct rNTP* (1 bound, 0 unbound).

(Important technical note: in the original draft,  $d_t$  was used both for binding and for a  $\pm$  direction label; we rename the binding variable to  $b_t$  throughout to avoid collisions and compilation errors. The  $\pm$  label will be introduced later as a separate symbol without reusing  $b_t$ .)

#### 2.3.3 Transition rates (rigorous definition via the generator)

Transitions from state  $s = (m, z, b)$  consist of the following three classes.

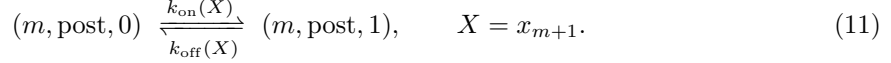
(i) Spontaneous pre/post fluctuations due to DNA structure (forward/backward bias)



To make a “DNA-structure origin” explicit, one can parametrize using a local structural free-energy difference  $\Delta G_{\text{struct}}$  as

$$\ln \frac{k_m^+}{k_m^-} = -\beta \Delta G_{\text{struct}}(x_m, x_{m+1}). \quad (10)$$

(ii) Binding/unbinding of the correct rNTP (occurs only in the post state)



The binding rate  $k_{\text{on}}(X)$  may be proportional to the concentration of the correct rNTP. Using an equilibrium binding free energy  $\Delta G_{\text{bind}}(X)$ , one may impose a local detailed-balance-type relation such as

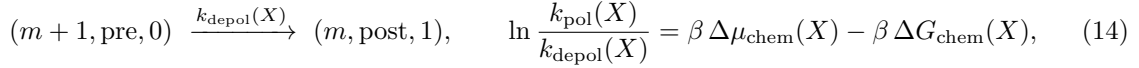
$$\ln \frac{k_{\text{on}}(X)}{k_{\text{off}}(X)} = -\beta \Delta G_{\text{bind}}(X) + \ln[\text{rNTP}(X)]. \quad (12)$$

(iii) Polymerization (locking) commitment: suppression of backward fluctuations = rectification From the post state with the correct rNTP bound, polymerization commits one base and advances to the next position:



In our stance, (13) does not mean “polymerization free energy mechanically pushes RNAP forward.” Rather, it models a rectification mechanism: the chemical reaction captures (locks) the moment RNAP resides in *post* under the mechanical fluctuations (9), making return from *post* to *pre* effectively less likely.

To retain mathematical rigor (domain of the path-space KL), we also introduce a minimal reverse reaction (depolymerization) corresponding to (13):



where  $\Delta \mu_{\text{chem}}(X)$  is the chemical potential difference for  $\text{NTP} \rightarrow \text{NMP} + \text{PP}_i$ . Under experimental conditions where the reverse reaction is negligible, one may assume  $k_{\text{depol}}(X) \ll k_{\text{pol}}(X)$ . (Equation (14) expresses that chemical driving contributes to dissipation; it is not an assumption of mechanical propulsion.)

**Generator** With the above, the CTMC on  $\mathcal{Y}$  is rigorously defined by the generator  $\mathcal{L}$ :

$$(\mathcal{L}f)(s) = \sum_{s' \neq s} k_{s \rightarrow s'} [f(s') - f(s)], \quad (15)$$

where  $k_{s \rightarrow s'}$  are given by (9), (11), (13) (and (14)).

### 2.3.4 Locking probability: rNTP binding suppresses backtracking and realizes forward motion

The most direct demonstration of “forward motion using DNA information” in this model is the probability that, upon entering the post state, polymerization commitment occurs before backward return ( $\text{post} \rightarrow \text{pre}$ ). From the unbound post state  $(m, \text{post}, 0)$ , binding (rate  $k_{\text{on}}(X)$ ) competes with backward return (rate  $k_m^-$ ); after binding, in  $(m, \text{post}, 1)$ , polymerization (rate  $k_{\text{pol}}(X)$ ) competes with unbinding (rate  $k_{\text{off}}(X)$ ). The probability that polymerization commitment (13) eventually occurs

after entering post, denoted  $p_{\text{lock}}(X)$ , can be written (even allowing unbinding) in an elementary form:

$$p_{\text{lock}}(X) = \frac{k_{\text{on}}(X) k_{\text{pol}}(X)}{k_{\text{on}}(X) k_{\text{pol}}(X) + k_m^-(k_{\text{pol}}(X) + k_{\text{off}}(X))}. \quad (16)$$

Thus, as the concentration of the correct rNTP increases and  $k_{\text{on}}(X)$  increases,  $p_{\text{lock}}(X)$  increases, backward return is suppressed, and forward progression is rectified. This rectification presupposes the DNA-structure-driven fluctuations (pre/post) via (10), and does not assume that polymerization free energy directly drives mechanical motion.

### 2.3.5 Path-space KL and dissipation

This CTMC determines  $P_{XY}$ , i.e. the joint path measure of  $X_t = x_{m_t+1}$  and  $Y_t = (m_t, z_t, b_t)$ . For time reversal ( $t \mapsto T - t$ ) starting from a stationary initial distribution  $\pi$ , a standard fact for CTMCs is that the entropy production (dissipation) rate can be written as

$$\dot{\Sigma}_{XY} = \sum_{s, s'} \pi_s k_{s \rightarrow s'} \ln \frac{k_{s \rightarrow s'}}{k_{s' \rightarrow s}}. \quad (17)$$

(see [2]). We also restate the same expression with a different label:

$$\dot{\Sigma}_{XY} = \sum_{s, s'} \pi_s k_{s \rightarrow s'} \ln \frac{k_{s \rightarrow s'}}{k_{s' \rightarrow s}}. \quad (18)$$

The interface dissipation is defined by (4) as  $\Sigma_{\text{int}} = \Sigma_{XY} - \frac{1}{2}(\Sigma_X + \Sigma_Y)$ , and is interpreted as the quantity extracting the irreversibility of RNAP conditioned on the template variable  $X_t$  (the  $P_{Y|X}$  side of (6)). In this model, since binding and polymerization rates are modulated through  $X = x_{m+1}$ , one generally can have  $\Sigma_{\text{int}} > 0$ .

### 2.3.6 Nontriviality of interface dissipation for fixed DNA

Even though the DNA sequence  $\mathbf{x}$  is quenched and fixed, the key reason  $\Sigma_{\text{int}}$  is generally nontrivial in this model is that we define the template-side variable as in (7), namely as the “next base” sampled by the RNAP position process  $m_t$ . Since  $m_t$  fluctuates as part of the CTMC,  $X_t = x_{m_t+1}$  becomes a stochastic process describing how RNAP scans the fixed string  $\mathbf{x}$ .

This renders the  $P_{Y|X}$  side in the conditional-KL representation (6) nontrivial. By treating  $X$  not as a static external parameter but as the input stream actually referenced at the interface, the statement “forward motion is rectified using nucleic-acid information” becomes quantifiable as conditional irreversibility.

### 2.3.7 Stationary flux and rectification: effective drift

Using the stationary distribution  $\pi_{mzb}$  of the CTMC on  $(m, z, b)$ , the firing rate per unit time of forward commitments is

$$r_+ = \sum_m \pi_{m,\text{post},1} k_{\text{pol}}(x_{m+1}), \quad (19)$$

and if the reverse reaction (depolymerization) is included, the firing rate of backward commitments is

$$r_- = \sum_m \pi_{m+1,\text{pre},0} k_{\text{depol}}(x_{m+1}). \quad (20)$$

Therefore, defining the long-time average effective drift (bases/s) by

$$v := \lim_{T \rightarrow \infty} \frac{\mathbb{E}[m_T - m_0]}{T} = r_+ - r_-, \quad (21)$$

rectification is expressed as  $v > 0$ .

### 2.3.8 Decomposition of total dissipation

The total dissipation rate (17) can be additively decomposed by transition class. Namely, separating contributions from (9), (11), (13) (and reverse reactions), one can write

$$\dot{\Sigma}_{XY} = \dot{\Sigma}_{\text{pre/post}} + \dot{\Sigma}_{\text{bind}} + \dot{\Sigma}_{\text{pol}}. \quad (22)$$

For example, the contribution from the polymerization subchannel is

$$\dot{\Sigma}_{\text{pol}} = \sum_m \pi_{m,\text{post},1} k_{\text{pol}}(x_{m+1}) \ln \frac{k_{\text{pol}}(x_{m+1})}{k_{\text{depol}}(x_{m+1})}, \quad (23)$$

which becomes an explicit contribution of chemical driving upon substituting (14).

Meanwhile, the contribution from the pre/post fluctuations (9) is

$$\dot{\Sigma}_{\text{pre/post}} = \sum_m \sum_{b \in \{0,1\}} \pi_{m,\text{pre},b} k_m^+ \ln \frac{k_m^+}{k_m^-} + \pi_{m,\text{post},b} k_m^- \ln \frac{k_m^-}{k_m^+}, \quad (24)$$

which, using (10), can be understood as dissipation due to asymmetry of fluctuations determined by local structural free-energy differences.

### 2.3.9 Time reversal and boundary terms

To use the path-space KL (2) rigorously for a CTMC, we define the time-reversal map for paths on  $[0, T]$  by  $\mathcal{R} : (s_t)_{t \in [0, T]} \mapsto (s_{T-t})_{t \in [0, T]}$ . (If there are odd variables, one includes sign flips; for  $s = (m, z, b)$  here, none are needed.) A standard identity yields

$$\Sigma_{XY} = \mathbb{E} \left[ \sum_{(s \rightarrow s') \in \omega} \ln \frac{k_{s \rightarrow s'}}{k_{s' \rightarrow s}} \right], \quad (25)$$

with boundary terms vanishing under stationary start or being  $o(T)$  (see [2]). Therefore, in numerical experiments, one can estimate  $\Sigma_{XY}$  by sampling trajectories generated by the Gillespie algorithm and averaging the jump-sum in (25).

### 2.3.10 Connection to numerical experiments (overview)

Numerical simulation of this model can be implemented in the following two steps:

1. **Simulation of the joint CTMC:** Generate the state  $s = (m, z, b)$  by the Gillespie algorithm, and for each jump along the trajectory, accumulate the increment  $\Delta \Sigma = \ln \frac{k_{s \rightarrow s'}}{k_{s' \rightarrow s}}$  to estimate  $\Sigma_{XY}$ .
2. **Estimation of marginal dissipations:** Since the marginal path measures  $P_X, P_Y$  are generally non-Markovian, estimate  $\Sigma_X, \Sigma_Y$  via finite-memory (higher-order Markov) approximation or an HMM approximation as log-likelihood ratios between forward and reverse, and then obtain  $\Sigma_{\text{int}} = \Sigma_{XY} - \frac{1}{2}(\Sigma_X + \Sigma_Y)$  (see Section 4 for details).

## 3 Numerical evaluation: velocity, dissipation, and interface dissipation in the locking-rectification CTMC

In this section, for the Brownian-ratchet CTMC defined in Section 2.3,  $Y_t = (m_t, z_t, b_t)$  and  $X_t = x_{m_t+1}$ , we provide a procedure to quantify, based on trajectory samples, (i) the effective drift (forward velocity), (ii) the total dissipation (path-space KL), and (iii) marginal dissipations and interface dissipation. The numerical evaluation used here is written in a unified way as a method for estimating the log-likelihood ratio of forward versus reverse path measures, based on standard trajectory representations of CTMCs.

### 3.1 Finite-length system and stationarization

To stably evaluate long-time-limit dissipation rates, we treat the position  $m$  as an irreducible process on a finite set. For computational convenience we adopt periodic boundary conditions (a ring) and set

$$m \in \{1, \dots, L\}, \quad m + 1 \equiv 1 \ (m = L) \quad (26)$$

(which guarantees a unique stationary distribution). For trajectories on the time interval  $[0, T]$ , we use the portion after discarding a sufficiently long burn-in time  $T_{\text{burn}}$ .

### 3.2 Specific parametrizations of transition rates

For the transitions (9), (11), and (13) of Section 2.3, the numerical evaluation uses the following parameterizations.

#### (i) pre/post fluctuations (structural free-energy difference)

$$k_m^+ = k_0 \exp\left[-\frac{\beta}{2} \Delta G_{\text{struct}}(x_m, x_{m+1})\right], \quad k_m^- = k_0 \exp\left[+\frac{\beta}{2} \Delta G_{\text{struct}}(x_m, x_{m+1})\right]. \quad (27)$$

This enforces  $\ln \frac{k_m^+}{k_m^-} = -\beta \Delta G_{\text{struct}}(x_m, x_{m+1})$ . A forward/backward ratio  $\simeq 3:1$  corresponds to the specialization  $\Delta G_{\text{struct}} \equiv -k_B T \ln 3$ .

(ii) Binding/unbinding of the correct rNTP (dependence on  $X = x_{m+1}$ ) Binding/unbinding occurs only in the post state:

$$k_{\text{on}}(X) = k_{\text{on}}^0 c_X, \quad k_{\text{off}}(X) = k_{\text{off}}^0 \exp[+\beta \Delta G_{\text{bind}}(X)], \quad (28)$$

where  $c_X \propto [\text{rNTP}(X)]$  is the input concentration (or its nondimensionalization).

(iii) Polymerization (locking) and reverse reaction (depolymerization) To define the path-space KL rigorously, we introduce a minimal reverse reaction for polymerization:

$$k_{\text{pol}}(X) = k_{\text{pol}}^0 \exp[-\beta \Delta G_{\text{act}}(X)], \quad k_{\text{depol}}(X) = k_{\text{pol}}(X) \exp[-\beta(\Delta \mu_{\text{chem}} - \Delta G_{\text{chem}}(X))]. \quad (29)$$

In regimes where the reverse reaction is negligible, one may set  $k_{\text{depol}}(X) \ll k_{\text{pol}}(X)$ .

### 3.3 Definition of observables

#### 3.3.1 Velocity (effective drift)

Count the number of polymerization commitments  $N_+(T)$  and depolymerization events  $N_-(T)$ , and define

$$M_T := N_+(T) - N_-(T), \quad v := \lim_{T \rightarrow \infty} \frac{\mathbb{E}[M_T]}{T}. \quad (30)$$

For finite-time estimation, use  $v \approx M_T/T$ .

#### 3.3.2 Total (joint) dissipation

Under stationary start, for a trajectory  $\omega$  with jump sequence, evaluate

$$\Sigma_{XY}(\omega) = \sum_{(s \rightarrow s') \in \omega} \ln \frac{k_{s \rightarrow s'}}{k_{s' \rightarrow s}}, \quad \dot{\Sigma}_{XY} \approx \frac{\Sigma_{XY}(\omega)}{T}. \quad (31)$$

In this model, the jump increments are explicit:

- pre  $\rightarrow$  post:  $\Delta \Sigma = \ln \frac{k_m^+}{k_m^-} = -\beta \Delta G_{\text{struct}}(x_m, x_{m+1})$ ,
- post  $\rightarrow$  pre:  $\Delta \Sigma = +\beta \Delta G_{\text{struct}}(x_m, x_{m+1})$ ,
- binding:  $\Delta \Sigma = \ln \frac{k_{\text{on}}(X)}{k_{\text{off}}(X)}$ ; unbinding has the opposite sign,
- polymerization:  $\Delta \Sigma = \ln \frac{k_{\text{pol}}(X)}{k_{\text{depol}}(X)}$ ; depolymerization has the opposite sign.

### 3.3.3 Marginal dissipations and interface dissipation

$$\dot{\Sigma}_X := \lim_{T \rightarrow \infty} \frac{1}{T} D_{\text{KL}}(P_X \parallel P_X^{\text{R}}), \quad \dot{\Sigma}_Y := \lim_{T \rightarrow \infty} \frac{1}{T} D_{\text{KL}}(P_Y \parallel P_Y^{\text{R}}), \quad \dot{\Sigma}_{\text{int}} := \dot{\Sigma}_{XY} - \frac{1}{2}(\dot{\Sigma}_X + \dot{\Sigma}_Y). \quad (32)$$

Since the marginal path measures  $P_X, P_Y$  of  $X_t = x_{m_t+1}$  and  $Y_t = (m_t, z_t, b_t)$  are generally non-Markovian, we use a forward/reverse path-likelihood estimator to evaluate  $\dot{\Sigma}_X, \dot{\Sigma}_Y$ .

## 3.4 Trajectory generation (Gillespie) and simultaneous computation of total dissipation

For the state  $s = (m, z, b)$ , enumerate the possible transitions  $s \rightarrow s'$  and the rates  $k_{s \rightarrow s'}$ , and sample the next jump time and destination using the Gillespie algorithm. For each jump, add the increment  $\Delta \Sigma = \ln \frac{k_{s \rightarrow s'}}{k_{s' \rightarrow s}}$  in (31), and simultaneously record the number of polymerization and depolymerization events to evaluate the velocity in (30).

## 3.5 Estimating marginal dissipations: forward/reverse likelihood ratio

We estimate the KL of marginal path measures as a likelihood ratio between a model for the forward process and a model for the reverse process. Sample the CTMC trajectory at a fixed interval  $\Delta t$ :  $X_n := X_{n\Delta t}$ ,  $Y_n := Y_{n\Delta t}$ , and treat them as discrete-time sequences.

### 3.5.1 Finite-memory approximation

For the sequence  $X_0, X_1, \dots, X_N$ , construct a conditional distribution with memory length  $r$ ,  $\hat{p}_F(X_n \mid X_{n-1}, \dots, X_{n-r})$ , either by frequency estimation or parametric estimation ( $F$  denotes forward). For the reversed-order sequence  $X_N, \dots, X_0$ , construct similarly  $\hat{p}_R(\cdot \mid \cdot)$  ( $R$  denotes reverse). Then define the discrete-time approximate KL-rate estimator by

$$\hat{\dot{\Sigma}}_X := \frac{1}{N\Delta t} \sum_{n=r}^N \ln \frac{\hat{p}_F(X_n \mid X_{n-1}, \dots, X_{n-r})}{\hat{p}_R(X_n \mid X_{n-1}, \dots, X_{n-r})}. \quad (33)$$

(Analogously, obtain  $\hat{\dot{\Sigma}}_Y$  for the sequence  $Y$ .) Choose the memory length  $r$  appropriately by balancing stability and approximation error.

### 3.5.2 Estimating interface dissipation

Since the total dissipation rate can be evaluated directly from (31), estimate the interface dissipation rate by (32):

$$\hat{\dot{\Sigma}}_{\text{int}} := \hat{\dot{\Sigma}}_{XY} - \frac{1}{2}(\hat{\dot{\Sigma}}_X + \hat{\dot{\Sigma}}_Y). \quad (34)$$

## 4 Estimation of interface dissipation and numerical simulation (locking-rectification CTMC)

In this section, for the locking-rectification CTMC defined in Section 2.3, we provide a procedure to: (1) fix the forward/backward ratio (pre/post bias) identified from the literature or from single-molecule traces as input, (2) generate trajectories via the Gillespie algorithm and evaluate the total dissipation (path-space KL) exactly, and (3) numerically construct the interface dissipation  $\Sigma_{\text{int}} = \Sigma_{XY} - \frac{1}{2}(\Sigma_X + \Sigma_Y)$  by estimating marginal dissipations. The purpose of this section is to evaluate, from the same data set, the velocity  $v$ , the total dissipation rate  $\dot{\Sigma}_{XY}$ , the marginal dissipation rates  $\dot{\Sigma}_X, \dot{\Sigma}_Y$ , and the interface dissipation rate  $\dot{\Sigma}_{\text{int}}$  as quantities that can be plotted.

#### 4.1 Definition of observed series: $(X_t, Y_t)$ and the forward/backward label

The interface input and RNAP state in this manuscript are

$$X_t := x_{m_t+1}, \quad Y_t := (m_t, z_t, b_t), \quad (35)$$

(see (7)). Here  $z_t \in \{\text{pre, post}\}$  is the 1-nt translocation register, and  $b_t \in \{0, 1\}$  is the binding state of the correct rNTP.

To remain consistent with the notation in the prior work, we also represent the translocation state by a binary label

$$d_t := \begin{cases} + & (z_t = \text{post}), \\ - & (z_t = \text{pre}) \end{cases} \quad (36)$$

as well. Below, identification of the forward/backward ratio is equivalent whether we use  $z_t$  or  $d_t$ .

#### 4.2 Identification of the forward/backward ratio: estimating $K_\delta = k_{-1}/k_1$

In our locking-rectification model, the spontaneous translocation fluctuation on-path is written as

$$(m, \text{pre}, b) \xrightleftharpoons[k_{-1}(m)]{k_1(m)} (m, \text{post}, b). \quad (37)$$

Following the literature standard, we define the forward/backward ratio by

$$K_\delta(m) := \frac{\Pr(z = \text{pre} \mid m)}{\Pr(z = \text{post} \mid m)} = \frac{k_{-1}(m)}{k_1(m)}. \quad (38)$$

Given an observation time  $T$ , count at position  $m$  the occupation times  $T_{\text{pre}}(m), T_{\text{post}}(m)$  and the transition counts  $n_{\text{pre} \rightarrow \text{post}}(m), n_{\text{post} \rightarrow \text{pre}}(m)$ . Then, as the maximum-likelihood estimator for a two-state CTMC,

$$\hat{k}_1(m) = \frac{n_{\text{pre} \rightarrow \text{post}}(m)}{T_{\text{pre}}(m)}, \quad \hat{k}_{-1}(m) = \frac{n_{\text{post} \rightarrow \text{pre}}(m)}{T_{\text{post}}(m)}, \quad \hat{K}_\delta(m) = \frac{\hat{k}_{-1}(m)}{\hat{k}_1(m)} \quad (39)$$

is obtained. If a quasi-steady approximation is valid, one may also evaluate  $\hat{K}_\delta(m) \approx T_{\text{pre}}(m)/T_{\text{post}}(m)$  via the occupancy ratio.

In the numerical evaluations below, we adopt  $\hat{K}_\delta$  corresponding to the RNAP system of interest as input and fix the ratio of  $k_1, k_{-1}$  to (38). (If needed, one can make  $K_\delta(m)$  position dependent and treat it as a local structural bias.)

#### 4.3 Trajectory generation: Gillespie algorithm and simultaneous computation of total dissipation $\Sigma_{XY}$

The transition rates (9), (11), (13) (and the reverse reaction corresponding to (14)) define a CTMC on a finite state space. Generate a trajectory  $\omega$  over the interval  $[0, T]$  by the Gillespie algorithm. If starting from the stationary distribution, the total (joint) dissipation  $\Sigma_{XY}$  is given as the jump-sequence log ratio:

$$\Sigma_{XY}(\omega) = \sum_{(s \rightarrow s') \in \omega} \ln \frac{k_{s \rightarrow s'}}{k_{s' \rightarrow s}}. \quad (40)$$

Hence the total dissipation rate can be evaluated as  $\dot{\Sigma}_{XY} \approx \Sigma_{XY}(\omega)/T$ .

At the same time, count the number of polymerization commitments (13),  $N_+(T)$ , and the number of reverse reactions (depolymerizations),  $N_-(T)$ , and evaluate the effective drift (mean velocity) as

$$v \approx \frac{N_+(T) - N_-(T)}{T}. \quad (41)$$

#### 4.4 Estimating marginal dissipations $\Sigma_X, \Sigma_Y$ : forward/reverse likelihood ratio

The interface dissipation is

$$\Sigma_{\text{int}} = \Sigma_{XY} - \frac{1}{2}(\Sigma_X + \Sigma_Y). \quad (42)$$

Since the projected path measures  $P_X, P_Y$  are generally non-Markovian, we evaluate  $\Sigma_X, \Sigma_Y$  using estimators based on a forward/reverse likelihood ratio constructed from an effective conditional transition probability.

Sample the continuous-time trajectory  $(X_t, Y_t)$  at interval  $\Delta t$  and form discrete sequences:

$$X_n := X_{n\Delta t}, \quad Y_n := Y_{n\Delta t}, \quad n = 0, 1, \dots, N, \quad (43)$$

(where  $N\Delta t = T_{\text{eff}}$ ). Assume a finite memory length  $r$ , estimate from the forward sequence  $\hat{p}_F(X_{n+1} | X_{n-r+1:n})$ , and estimate from the time-reversed (reverse-order) sequence  $\hat{p}_R(X_{n+1} | X_{n-r+1:n})$ . Then define the estimator for the marginal dissipation rate (KL rate) by

$$\hat{\Sigma}_X^{(r)} = \frac{1}{N_{\text{eff}}\Delta t} \sum_{n=r-1}^{N-1} \ln \frac{\hat{p}_F(X_{n+1} | X_{n-r+1:n})}{\hat{p}_R(X_{n+1} | X_{n-r+1:n})}, \quad (44)$$

where  $N_{\text{eff}} := N - (r - 1)$ . Similarly obtain  $\hat{\Sigma}_Y^{(r)}$  from the  $Y$  sequence. One may also apply the same estimator to the joint sequence  $(X_n, Y_n)$  to compute  $\hat{\Sigma}_{XY}^{(r)}$ .

$$\hat{\Sigma}_S^{(r)} = \frac{1}{N_{\text{eff}}\Delta t} \sum_{n=r-1}^{N-1} \ln \frac{\hat{p}_F(S_{n+1} | S_{n-r+1:n})}{\hat{p}_R(S_{n+1} | S_{n-r+1:n})}, \quad S_n \in \{X_n, Y_n, (X_n, Y_n)\}. \quad (45)$$

(Equation (44) is the case  $S = X$ .)

Finally estimate the interface dissipation rate by

$$\hat{\Sigma}_{\text{int}}^{(r)} = \hat{\Sigma}_{XY}^{(r)} - \frac{1}{2} \left( \hat{\Sigma}_X^{(r)} + \hat{\Sigma}_Y^{(r)} \right). \quad (46)$$

Increasing  $r$  captures non-Markovianity more faithfully, but under finite samples it increases variance because the number of contexts grows rapidly; this can inflate dissipation estimates unless  $T$  is very large (or smoothing/coarse-graining is used).

#### 4.5 Quantities to plot

Using the identified forward/backward ratio  $\hat{K}_\delta$  as input, simulate the locking-rectification CTMC and evaluate/plot, under the same conditions:

1. mean velocity  $v$  (Eq. (41));
2. total dissipation rate  $\dot{\Sigma}_{XY}$  (Eq. (40));
3. marginal dissipation rates  $\dot{\Sigma}_X, \dot{\Sigma}_Y$  and the interface dissipation rate  $\dot{\Sigma}_{\text{int}}$  (Eqs. (44), (46)).

This enables comparison, within a single path-space KL bookkeeping, of (i) how the asymmetry of spontaneous pre/post fluctuations influences kinematics and irreversibility, and (ii) to what extent binding/polymerization (locking rectification) is extracted as interface dissipation.

#### 4.6 Convergence diagnostics for interface-dissipation estimation under finite samples: dependence on Markov order $r$

Sample the continuous-time trajectory at interval  $\Delta t$  to obtain  $X_n := X_{n\Delta t}$  and  $Y_n := Y_{n\Delta t}$ . Even if the underlying joint process is Markovian in continuous time, the projected sequences  $X_n$  and  $Y_n$  can exhibit history dependence (non-Markovianity). To quantify irreversibility from such sequences, approximate the path measure by an  $r$ th-order Markov model and estimate dissipation rates from the forward/reverse likelihood ratio.

**Quasi-stationary / quasi-periodic assumption.** In RNAP systems, templates can be repetitive, and within a single run input statistics may be approximately stationary. Our periodic boundary condition in simulations realizes this quasi-periodic repeated observation and makes the  $T$ -dependence of estimators interpretable under finite samples.

**Markov order  $r$ .** The Markov order  $r$  is the memory length in the discrete approximation:

$$p(s_{n+1} | s_{0:n}) \approx p^{(r)}(s_{n+1} | s_{n-r+1:n}).$$

**Estimator.** Using Eq. (47) below, construct  $\hat{\Sigma}^{(r)}$  for  $S = X$ ,  $S = Y$ , and  $S = (X, Y)$ , and then define  $\hat{\Sigma}_{\text{int}}^{(r)}$  by Eq. (48).

$$\hat{\Sigma}^{(r)} = \frac{1}{N_{\text{eff}} \Delta t} \sum_{n=r-1}^{N-1} \ln \frac{\hat{p}_{\text{F}}(s_{n+1} | s_{n-r+1:n})}{\hat{p}_{\text{R}}(s_{n+1} | s_{n-r+1:n})}, \quad s_n \in \{X_n, Y_n, (X_n, Y_n)\}, \quad (47)$$

where  $N_{\text{eff}} := N - (r - 1)$ . For each  $r$ , the interface-dissipation rate is

$$\hat{\Sigma}_{\text{int}}^{(r)} := \hat{\Sigma}_{XY}^{(r)} - \frac{1}{2} \left( \hat{\Sigma}_X^{(r)} + \hat{\Sigma}_Y^{(r)} \right). \quad (48)$$

**Bias-variance trade-off.** Increasing  $r$  reduces modeling bias (captures longer memory) but increases variance because contexts become sparse; this can inflate the log-likelihood ratio in finite samples. Accordingly, we use  $r = 1$  as a stable baseline and interpret  $r \geq 2$  primarily as a diagnostic of history dependence unless  $T$  is very large (or coarse-graining/smoothing is introduced).

## 4.7 Calibration of coarse-grained motion: drift $\mu$ and diffusion $D$

In analyses of single-molecule traces and prior work, the transcription length is often modeled as a coarse-grained 1D motion characterized by a drift  $\mu$  and a diffusion coefficient  $D$ . Here we use the number of polymerization commitments  $M(t) = N_+(t) - N_-(t)$  as a proxy and identify  $\mu$  and  $D$  via

$$\mathbb{E}[M(t)] \simeq \mu t, \quad \text{Var}[M(t)] \simeq 2Dt. \quad (49)$$

Generate many independent trajectories, evaluate  $\mathbb{E}[M(t)]$  and  $\text{Var}[M(t)]$  at equally spaced times, and estimate  $\mu$  and  $D$  via linear regression:

$$\mathbb{E}[M(t)] \approx \hat{\mu} t + \text{const.}, \quad \text{Var}[M(t)] \approx 2\hat{D}t + \text{const.} \quad (50)$$

## 4.8 Literature background for the coarse-grained motion indicator $\mu/D$ , and the estimator used in this manuscript

For a coarse-grained position process  $m(t) \in \mathbb{Z}$  (1 step per 1 nt), define

$$\mu := \lim_{t \rightarrow \infty} \frac{d}{dt} \mathbb{E}[m(t)], \quad D := \lim_{t \rightarrow \infty} \frac{1}{2} \frac{d}{dt} \text{Var}[m(t)]. \quad (51)$$

A dimensionless indicator is  $\mu/D$ .

**Relation to the randomness parameter.** The randomness parameter is

$$r \equiv \frac{2D}{vd}, \quad (52)$$

where  $d$  is the step size [15]. Here  $d = 1$  (nt) and  $v = \mu$ , hence

$$\frac{\mu}{D} = \frac{2}{r}. \quad (53)$$

For a single-step Poisson renewal process,  $r = 1$  gives  $\mu/D = 2$ .

**Typical ranges in RNAP modeling.** One framework defines

$$\gamma := \frac{\langle t^2 \rangle - \langle t \rangle^2}{\langle t \rangle^2}, \quad (54)$$

and gives

$$D = \frac{\gamma}{2\langle t \rangle} \quad (55)$$

[16]. With  $\mu = 1/\langle t \rangle$ , one has

$$\frac{\mu}{D} = \frac{2}{\gamma}. \quad (56)$$

**Estimator for  $\mu/D$ .** Sample at interval  $\Delta t$  to form  $m_n := m(n\Delta t)$  (right-continuous sampling). Using increments  $\Delta m_n := m_{n+1} - m_n$ , compute

$$\widehat{\mu} := \frac{\overline{\Delta m}}{\Delta t}, \quad \widehat{D} := \frac{\text{Var}(\Delta m)}{2\Delta t}, \quad \widehat{\mu/D} := \frac{\widehat{\mu}}{\widehat{D}}. \quad (57)$$

In Fig. 6, vary  $\widehat{\mu/D}$  via parameter sweeps (e.g. scaling  $k_{\text{pol}}$ ), and for each condition plot the estimated interface dissipation rate against  $\widehat{\mu/D}$ .

## 5 Dictionary between prior $P(m, d, N)$ and the present $(X, Y), \Sigma_{\text{int}}$

In this section, we relate the previously used state variables  $(m, d, N)$  and the state function  $P(m, d, N)$  to the present interface input  $X_t := x_{m_t+1}$  and RNAP state  $Y_t := (m_t, z_t, b_t)$  (with  $z_t \in \{\text{pre, post}\}$  and  $b_t \in \{0, 1\}$ ). The bound state  $b_t = 1$  always denotes “binding of the correct rNTP.”

### 5.1 Definition: $(m, d, N)$ as an observation map and $P(m, d, N)$

**Definition 3** (Projection to the variables used previously). Given the present state  $Y_t = (m_t, z_t, b_t)$  and the fixed sequence  $\mathbf{x}$ , define the previously used observed variables  $(m_t, d_t, N_t)$  by

$$m_t := m_t, \quad d_t := \begin{cases} + & (z_t = \text{post}) \\ - & (z_t = \text{pre}) \end{cases}, \quad N_t := x_{m_t+1} =: X_t. \quad (58)$$

**Definition 4** (Meaning of the prior state function in the present manuscript). Under a stationary state, define the marginal distribution at time  $t$  by

$$P(m, d, N) := \Pr((m_t, d_t, N_t) = (m, d, N)), \quad (59)$$

which is time-independent in stationarity.

### 5.2 Proposition 1: the prior description is a coarse-graining of the present one, and dissipation obeys data processing

**Proposition 5** (Inclusion by coarse-graining and monotonicity of dissipation). *By Definition 3, the prior path measure is expressed as the pushforward of the present path measure. Hence, dissipation defined by path-space KL satisfies*

$$\Sigma_{mdN} := D_{\text{KL}}(P_{mdN} \parallel P_{mdN}^{\text{R}}) \leq D_{\text{KL}}(P_{XY} \parallel P_{XY}^{\text{R}}) =: \Sigma_{XY}. \quad (60)$$

*Proof.* KL divergence does not increase under a measurable map (data-processing inequality).  $\square$

### 5.3 Proposition 2: identifying the forward/backward ratio (a formula for plugging in numbers from data)

In this manuscript, the 1-nt pre/post fluctuation is written as pre  $\xrightleftharpoons[k_{-1}]{k_1}$  post, and following the literature standard we use the forward/backward ratio

$$K_\delta := \frac{[\text{pre}]}{[\text{post}]} = \frac{k_{-1}}{k_1} \quad (61)$$

(e.g., for yeast Pol II,  $K_\delta = 4.6$  has been reported). We provide a formula to identify this  $K_\delta$  from single-molecule traces.

**Proposition 6** (Estimating  $K_\delta$  from occupation times and transition counts). *Assume  $z_t \in \{\text{pre}, \text{post}\}$  is observable (or can be reconstructed by an HMM). Over a total observation time  $T$ , count the occupation times  $T_{\text{pre}}, T_{\text{post}}$  and the transition counts  $n_{\text{pre} \rightarrow \text{post}}, n_{\text{post} \rightarrow \text{pre}}$ . Then, as the maximum-likelihood estimator for a two-state CTMC,*

$$\hat{k}_1 = \frac{n_{\text{pre} \rightarrow \text{post}}}{T_{\text{pre}}}, \quad \hat{k}_{-1} = \frac{n_{\text{post} \rightarrow \text{pre}}}{T_{\text{post}}}, \quad \hat{K}_\delta = \frac{\hat{k}_{-1}}{\hat{k}_1} = \frac{n_{\text{post} \rightarrow \text{pre}} T_{\text{pre}}}{n_{\text{pre} \rightarrow \text{post}} T_{\text{post}}}. \quad (62)$$

Moreover, if a quasi-steady (fast pre/post) approximation is valid, one may evaluate

$$\hat{K}_\delta \approx \frac{T_{\text{pre}}}{T_{\text{post}}} \quad (63)$$

via the occupancy ratio.

*Proof.* Maximizing the likelihood of a two-state CTMC yields each directional rate as “transition count / occupation time.”  $\square$

By Proposition 6, the “forward/backward ratio” in the prior work can be numerically identified from real data as  $\hat{K}_\delta$ , and that value can be directly substituted into the present simulation parameters  $(k_1, k_{-1})$ .

## 6 Discussion: meaning of interface dissipation in the locking-rectification model

In this manuscript we applied the swap-symmetric *interface dissipation*  $\Sigma_{\text{int}} = \Sigma_{XY} - \frac{1}{2}(\Sigma_X + \Sigma_Y)$  to the composite DNA-template–RNAP system [1]. We formulated, as a continuous-time Markov jump process (CTMC), a minimal Brownian-ratchet mechanism: RNAP exhibits spontaneous translocation fluctuations (pre/post round trips) originating from DNA structure, while binding and polymerization of the correct rNTP capture the post state and thereby rectify the fluctuations [2, 14]. Within this framework, the forward/backward ratio  $K_\delta = k_{-1}/k_1$  is treated as an input identified from the literature or from single-molecule traces, and we provided a unified procedure to evaluate, from the same trajectory dataset, the velocity, total dissipation, marginal dissipations, and the interface dissipation.

### 6.1 Novel contributions of this work

The main contributions can be summarized as follows:

1. **Observer/observed-label-independent irreversibility.** Because  $\Sigma_{\text{int}}$  is invariant under swapping  $X \leftrightarrow Y$ , it provides a comparison axis that does not depend on how the “device” and the “target” are labeled [1].
2. **Isolating interface-origin irreversibility beyond mutual-information bookkeeping.** Interface dissipation directly quantifies the irreversibility of *conditional fluctuations generated by the interface* [1].

3. **A single swap-invariant handle on sequence-dependent RNAP kinetics.** This organizes previous “information term” interpretations (e.g. involving  $k_B T \log P(N)$ ) into a higher-level structure: interface dissipation plus gauge-dependent bookkeeping [7, 1].
4. **A practical estimation protocol for single-molecule data.** Total dissipation can be evaluated exactly as a CTMC jump-sum [2, 3], while marginal dissipations can be estimated via forward/reverse likelihood ratios using finite-memory models or HMM-based state inference when needed [6].
5. **Swap-invariant reinterpretation of “information-to-motion” narratives.** We focus on irreversibility that remains regardless of which subsystem is viewed as the observer, captured by  $\Sigma_{\text{int}}$  [1, 7].

## 6.2 Role of the forward/backward ratio $K_\delta$

The ratio  $K_\delta$  is a kinematic parameter characterizing the asymmetry of translocation fluctuations, introduced in the minimal model as the ratio in  $(m, \text{pre}, b) \xrightleftharpoons[k_{-1}]{k_1} (m, \text{post}, b)$ . Crucially,  $K_\delta$  alone does not determine a positive forward velocity. A net drift emerges only when fluctuations are rectified through competition with chemical capture processes (binding and polymerization of the correct rNTP) [14]. In that regime, the interface dissipation  $\Sigma_{\text{int}}$  increases not because of the *structural translocation fluctuations themselves*, but because the *capture strength is modulated by the template input  $X = x_{m+1}$*  [1]. Thus,  $K_\delta$  controls the *supply/attempt frequency* of fluctuations for rectification, whereas  $\Sigma_{\text{int}}$  captures the *input-dependent locking/rectification*.

## 6.3 Physical meaning of interface dissipation: “information-rectification cost”

Using the conditional-KL representation (6),  $\Sigma_{\text{int}}$  is interpreted as the (symmetrized) average irreversibility of RNAP fluctuations *conditioned on a fixed input  $X$*  [1]. As long as binding/polymerization rates depend on  $X$ , the statistics of post capture are modulated by the input, and this modulation remains as irreversibility in the conditional path measure. In this sense,  $\Sigma_{\text{int}}$  isolates the irreversibility associated with *input-dependent rectification via correct-rNTP capture*.

Meanwhile, input-independent internal chemical cycles are absorbed into the marginal dissipation  $\Sigma_Y$ , so  $\Sigma_{\text{int}}$  provides a bookkeeping that separates *internal* versus *interface (input-dependent)* dissipation [1]. This directly addresses the fact that traditional information-thermodynamic accounting can depend on the observer/observed partition.

## 6.4 Limitations and extensions

The minimal model was chosen to make “fluctuations + capture (locking) rectification” explicit. Pauses, long backtracking, and multiple pause pathways can be incorporated by extending the effective RNAP state space  $Y$ , without changing the definition or swap symmetry of  $\Sigma_{\text{int}} = \Sigma_{XY} - \frac{1}{2}(\Sigma_X + \Sigma_Y)$  [1]. Hence the same accounting applies at whatever resolution is required by data.

## 6.5 Summary

Under the minimal locking-rectification CTMC, we provided a consistent framework that (i) identifies  $K_\delta$  from data and uses it as an input, (ii) evaluates the total dissipation exactly as a jump-sum [2, 3], and (iii) estimates marginal dissipations via forward/reverse likelihood ratios to construct the interface dissipation [1]. Beyond RNAP, this suggests that interface dissipation functions as a partition-independent irreversibility indicator for molecular machines that rectify fluctuations through input-dependent capture [4].

## References

- [1] T. Tsuruyama, Thermodynamics Reconstructed from Information Theory: An Axiomatic Framework via Information-Volume Constraints and Path-Space KL Divergence, arXiv:2512.24655 (2025).
- [2] U. Seifert, Stochastic thermodynamics, fluctuation theorems and molecular machines, *Rep. Prog. Phys.* **75**, 126001 (2012).
- [3] J. Schnakenberg, Network theory of microscopic and macroscopic behavior of master equation systems, *Rev. Mod. Phys.* **48**, 571–585 (1976).
- [4] J. L. Lebowitz and H. Spohn, A Gallavotti–Cohen-type symmetry in the large deviation functional for stochastic dynamics, *J. Stat. Phys.* **95**, 333–365 (1999).
- [5] D. T. Gillespie, Exact stochastic simulation of coupled chemical reactions, *J. Phys. Chem.* **81**, 2340–2361 (1977).
- [6] L. R. Rabiner, A tutorial on hidden Markov models and selected applications in speech recognition, *Proc. IEEE* **77**, 257–286 (1989).
- [7] T. Tsuruyama, RNA polymerase is a unique Maxwell’s demon that converts its transcribing genetic information to free energy for its movement, *Eur. Phys. J. Plus* **138**, 604 (2023).
- [8] T. Tsuruyama, Thermodynamics of Information: Mutual Entropy in RNA Polymerase and Nanopore Sequencing, (Review manuscript / draft; see also related discussion in [7]).
- [9] E. A. Abbondanzieri, W. J. Greenleaf, J. W. Shaevitz, R. Landick, and S. M. Block, Direct observation of base-pair stepping by RNA polymerase, *Nature* **438**, 460–465 (2005).
- [10] P. Thomen, P. J. Lopez, U. Bockelmann, J. Guillerez, M. Dreyfus, and F. Heslot, T7 RNA polymerase studied by force measurements varying cofactor concentration, *Biophys. J.* **95**, 2423–2433 (2008).
- [11] L. Bai, R. M. Fulbright, and M. D. Wang, Mechanochemical kinetics of transcription elongation, *Phys. Rev. Lett.* **98**, 068103 (2007).
- [12] L. Bai, A. Shundrovsky, and M. D. Wang, Sequence-dependent kinetic model for transcription elongation by RNA polymerase, *J. Mol. Biol.* **344**, 335–349 (2004).
- [13] M. D. Wang, T. E. Elston, R. Landick, and S. M. Block, Force generation in RNA polymerase, *Science* **282**, 902–907 (1998).
- [14] Q. Guo and R. Sousa, Translocation by T7 RNA polymerase: a sensitively poised Brownian ratchet, *J. Mol. Biol.* **358**, 241–254 (2006).
- [15] P. Pietzonka and U. Seifert, Universal trade-off between power, efficiency, and constancy in steady-state heat engines, *Phys. Rev. Lett.* **120**, 190602 (2018).
- [16] V. Tripathi, G. M. Schütz, and D. Chowdhury, Interacting RNA polymerase motors on a DNA track: effects of traffic congestion and intrinsic noise, *Phys. Rev. E* **79**, 011921 (2009).

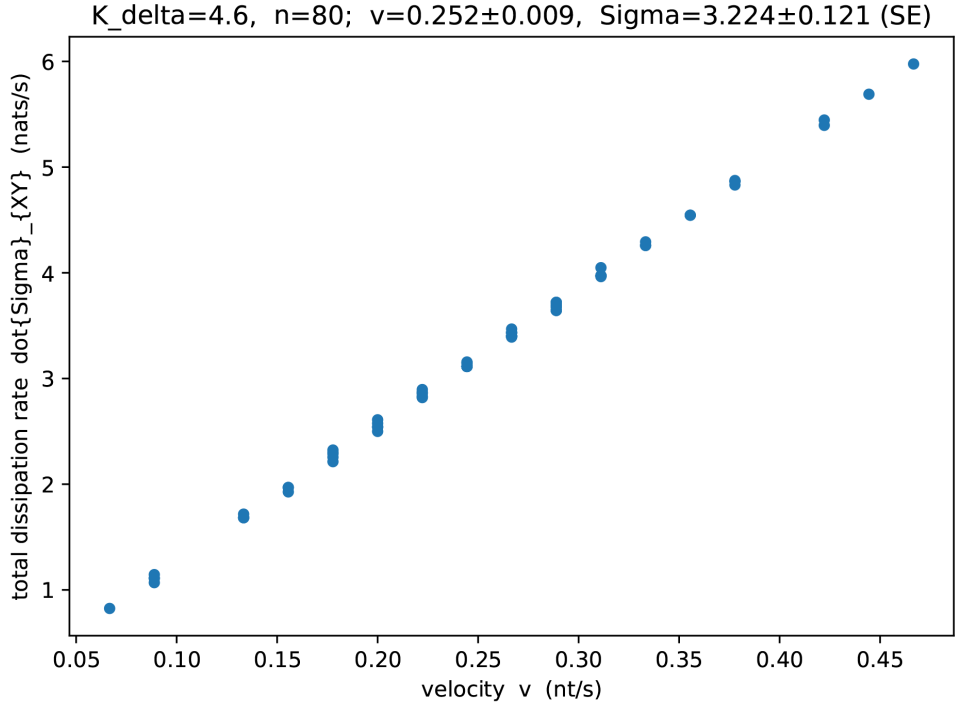


Figure 1: Simultaneous estimation of the mean velocity and total dissipation rate in the locking-rectification CTMC. RNAP translocation fluctuations between pre/post conformations are modeled as  $(m, \text{pre}, b) \rightleftharpoons (m, \text{post}, b)$ , with the forward/backward rate ratio  $K_\delta := k_{-1}/k_1$  fixed from the literature (or single-molecule traces). Binding/unbinding of the correct rNTP occurs only in the post state,  $(m, \text{post}, 0) \rightleftharpoons (m, \text{post}, 1)$ , and polymerization commitment after binding induces  $(m, \text{post}, 1) \rightarrow (m+1, \text{pre}, 0)$  (with depolymerization included as a minimal reverse process for mathematical consistency). Each marker corresponds to one Gillespie trajectory with effective observation time  $T_{\text{eff}} = T - T_{\text{burn}}$ . The velocity is estimated from the polymerization and depolymerization counts as  $v := (N_+ - N_-)/T_{\text{eff}}$  and the dissipation rate is reported as  $\dot{\Sigma}_{XY} := \Sigma_{XY}/T_{\text{eff}}$  (Eq. (40)). The scatter reflects finite-time and finite-sampling trajectory fluctuations.

Simultaneous estimation of the mean velocity and total dissipation rate in the locking-rectification CTMC. RNAP translocation fluctuations between pre/post conformations are modeled as  $(m, \text{pre}, b) \rightleftharpoons (m, \text{post}, b)$ , with the forward/backward rate ratio  $K_\delta := k_{-1}/k_1$  fixed from the literature (or single-molecule traces). Binding/unbinding of the correct rNTP occurs only in the post state,  $(m, \text{post}, 0) \rightleftharpoons (m, \text{post}, 1)$ , and polymerization commitment after binding induces  $(m, \text{post}, 1) \rightarrow (m+1, \text{pre}, 0)$  (with depolymerization included as a minimal reverse process for mathematical consistency).

Each marker corresponds to one Gillespie trajectory with effective observation time  $T_{\text{eff}} = T - T_{\text{burn}}$ . The velocity is estimated from the polymerization and depolymerization counts as  $v := (N_+ - N_-)/T_{\text{eff}}$  (Eq. (41)). The total dissipation along a trajectory  $\omega$  is computed from the CTMC path-likelihood ratio,  $\Sigma_{XY}(\omega) = \sum_{s \rightarrow s' \in \omega} \ln(k_{s \rightarrow s'}/k_{s' \rightarrow s})$ , and the dissipation rate is reported as  $\dot{\Sigma}_{XY} := \Sigma_{XY}/T_{\text{eff}}$  (Eq. (40)). The scatter reflects finite-time and finite-sampling trajectory fluctuations.

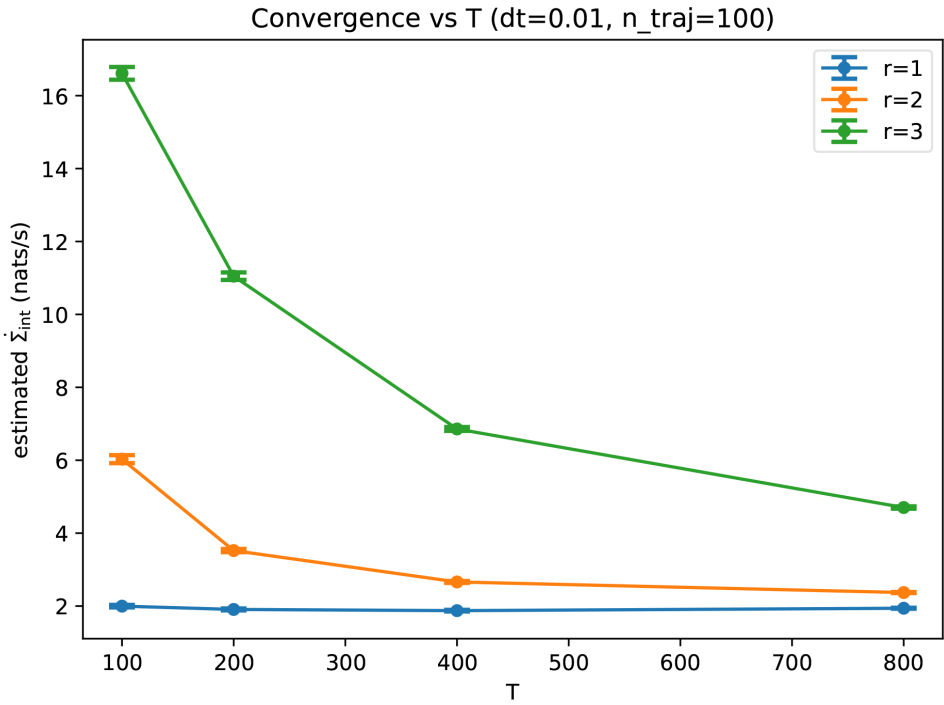


Figure 2: Convergence diagnostics for the interface-dissipation-rate estimator. With fixed sampling interval  $\Delta t$ , estimate  $\hat{\Sigma}_{\text{int}}^{(r)}$  for multiple Markov orders  $r$ , and plot the mean estimate as a function of observation length  $T$ . The result illustrates that  $r = 1$  is stable, whereas  $r \geq 2$  is more susceptible to sparse-estimation effects in finite data.

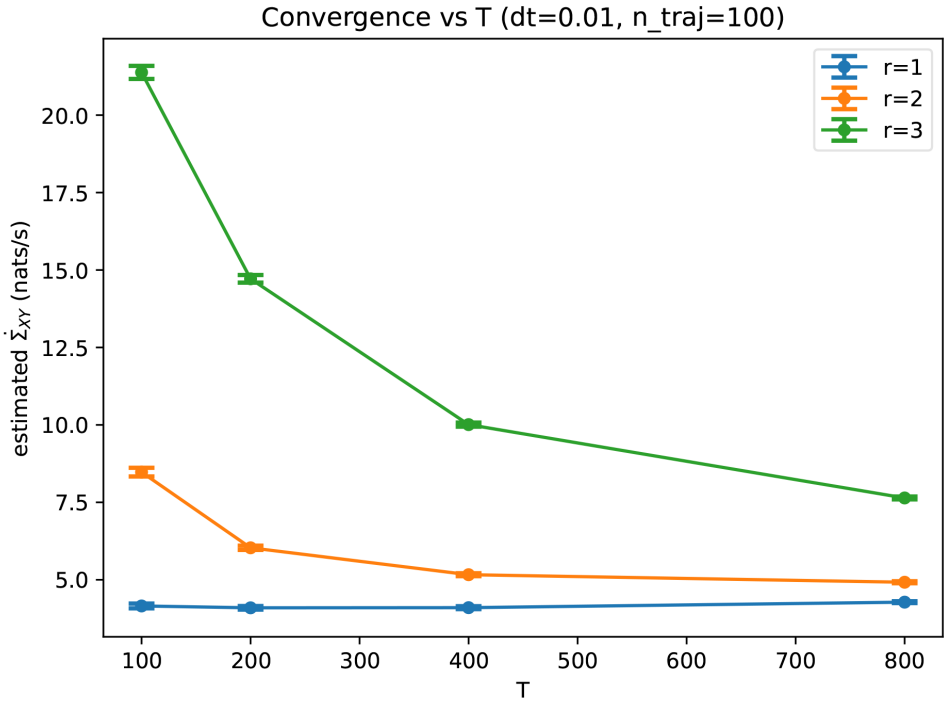


Figure 3: Convergence diagnostics for the total dissipation rate estimator. Under the same settings, estimate  $\hat{\Sigma}_{XY}^{(r)}$  (corresponding to  $S = (X, Y)$  in Eq. (45)) and compare across observation lengths  $T$ .

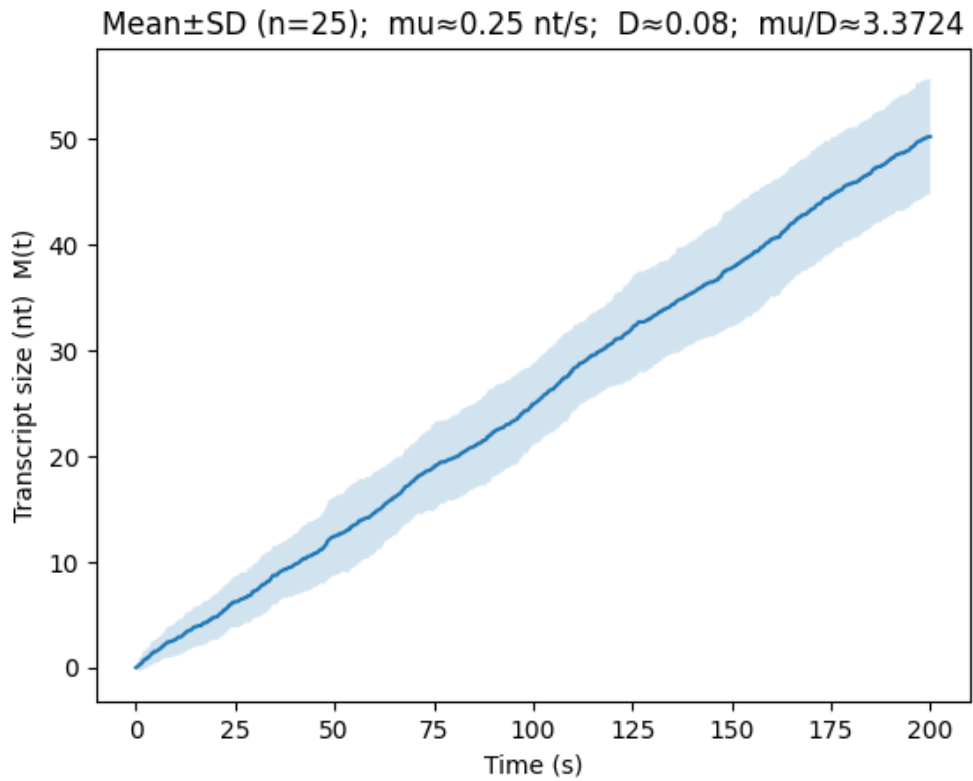


Figure 4: Transcription-length trajectories of the locking-rectification CTMC. Define  $M(t) = N_+(t) - N_-(t)$  as a proxy for transcription length, and evaluate  $\mathbb{E}[M(t)]$  (solid line) and  $\pm 1$  SD (shaded band) from many independent trajectories. Estimate the drift  $\mu$  via the linear regression in Eq. (50).

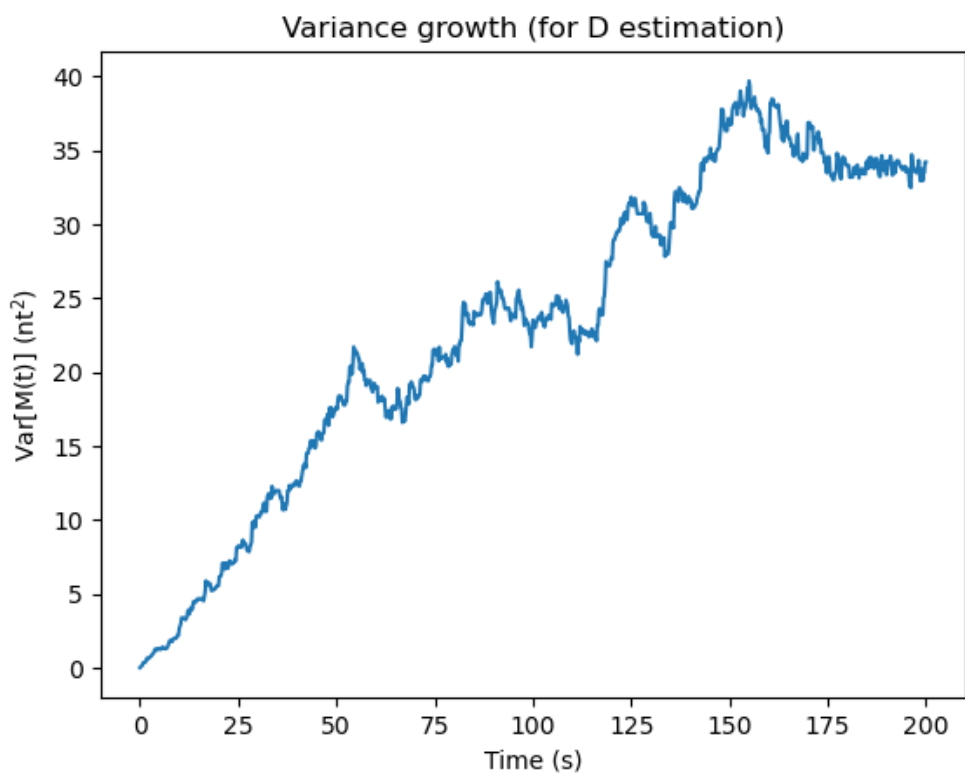


Figure 5: Estimating the diffusion coefficient via variance growth. From the same set of trajectories, evaluate  $\text{Var}[M(t)]$  and estimate  $D$  based on  $\text{Var}[M(t)] \simeq 2Dt$ .

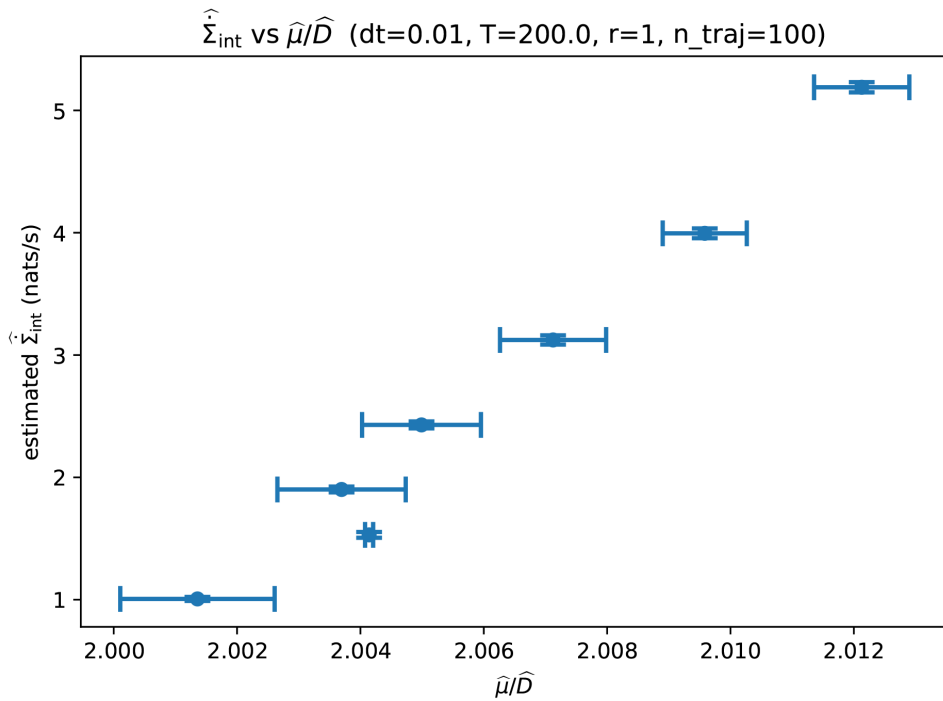


Figure 6: Relation between the interface dissipation rate and coarse-grained motion. From the discrete series  $(X_n, Y_n)$ , estimate  $\widehat{\Sigma}_{XY}$ ,  $\widehat{\Sigma}_X$ ,  $\widehat{\Sigma}_Y$  via forward/reverse likelihood ratios, and construct the interface dissipation rate via Eq. (45) and Eq. (46). Plot  $\widehat{\Sigma}_{\text{int}}$  as a function of  $\mu/D$  obtained from parameter sweeps.